J. Ocean Univ. China (Oceanic and Coastal Sea Research)
DOI 10.1007/s11802-011-1788-3
ISSN 1672-5182, 2011 10 (1): 1-8
http://www.ouc.edu.cn/xbywb/
E-mail:xbywb@ouc.edu.cn

Doctor Forum

A FVCOM-Based Unstructured Grid Wave, Current, Sediment Transport Model, I. Model Description and Validation

WU Lunyu[1), 2)], CHEN Changsheng[3), 4)], GUO Peifang[1), *], SHI Maochong[1)], QI Jianhua[3)], and GE Jianzhong[4)]

1) *Physical Oceanography Laboratory*, *Ocean University of China*, *Qingdao* 266100, *P. R. China*
2) *First Institute of Oceanography*, *State Oceanic Administration*, *Qingdao* 266061, *P. R. China*
3) *School for Marine Science and Technology*, *University of Massachusetts-Dartmouth*, *New Bedford*, *Massachusetts*, *USA*
4) *State Key Laboratory of Estuarine and Coastal Research*, *East China Normal University*, *Shanghai* 200062, *P. R. China*

(Received July 15, 2010; revised September 25, 2010; accepted October 29, 2010)

Abstract An effort was made to couple FVCOM (a three-dimensional (3D), unstructured grid, Finite Volume Coastal Ocean Model) and FVCOM-SWAVE (an unstructured grid, finite-volume surface wave model) for the study of nearshore ocean processes such as tides, circulation, storm surge, waves, sediment transport, and morphological evolution. The coupling between FVCOM and FVCOM-SWAVE was achieved through incorporating 3D radiation stress, wave-current-sediment-related bottom boundary layer, sea surface stress parameterizations, and morphology process. FVCOM also includes a 3D sediment transport module. With accurate fitting of irregular coastlines, the model provides a unique tool to study sediment dynamics in coastal ocean, estuaries, and wetlands where local geometries are characterized by inlets, islands, and intertidal marsh zones. The model was validated by two standard benchmark tests: 1) spectral waves approaching a mild sloping beach and 2) morphological changes of seabed in an idealized tidal inlet. In Test 1, model results were compared with both analytical solutions and laboratory experiments. A further comparison was also made with the structured grid Regional Ocean Model System (ROMS), which provides an insight into the performance of the two models with the same open boundary forcing.

Key words FVCOM; coupling; radiation stress; wave-current-sediment-related bottom boundary layer; morphology

1 Introduction

Nearshore ocean processes feature strong non-linear interactions of tides, winds, high-frequent surface waves, and river discharges. For example, the sedimentation, sediment resuspension, and morphological changes of the seabed in shallow water are directly controlled by the interaction of currents and waves through radiation stress and bottom boundary layer dynamics (Longuet-Higgins and Stewart, 1960; Longuet-Higgins 1970a, b; Grant and Medsen, 1979). Because the interaction is highly nonlinear and significantly varies in space and time, it is imperative that we develop a fully coupled hydrodynamics-wave-sediment model to understand this complex system.

Many efforts have been made to develop coupled current-wave models (Xie *et al.*, 2001; Moon, 2005; Sørensen *et al.*, 2006;Warner *et al.*, 2008; Liang *et al.*, 2007; Liu and Xie, 2009; Tang *et al.*, 2009). Most of these models are three-dimensional, structured grid models while unstructured grid models are usually two-dimensional. The most energetic areas of current-wave interactions appear in coastal oceans where local geometry is characterized by complex coastlines with islands, inlets, estuaries, and tidal marshes. Due to poor resolving of the reality of coastal geometry, structured grid models have limitation to simulate the geometrically controlled nearshore dynamic processes. The importance of resolving coastal geometry was studied in previous papers (Chen *et al.*, 2007), and a state-of-the-art unstructured grid, finite-volume, coastal ocean model (FVCOM) was developed to overcome the shortcomings associated with structured grid coastal ocean models (Chen *et al.*, 2003, 2006a, b). The finite-volume algorithm used in FVCOM has combined the flexibility of geometric fitting of finite element models and the computational efficiency of finite-difference models (Chen *et al.*, 2003; Huang *et al.*, 2008). FVCOM is suitable for coastal and estuarine applications.

This paper describes the algorithms used to couple a spectrum-based surface wave model with FVCOM. The surface wave model, FVCOM-SWAVE, is the unstructured grid version of SWAN (Simulating Waves Nearshore) developed by Qi *et al.* (2009). The model results were validated against some standard benchmark tests,

* Corresponding author. Tel: 0086-532-82032759
E-mail: pfguo@ouc.edu.cn

and compared with analytical solutions, laboratory experiments, and the Regional Ocean Model System (ROMS) (Haidvogel *et al.*, 2008; Warner *et al.*, 2008).

The following sections are organized as follows. The governing equations of FVCOM and FVCOM-SWAVE are described in Section 2. The finite-volume discrete algorithms for a two-way coupling between FVCOM and FVCOM-SWAVE are given in Section 3. The validation experiments are presented in Section 4, and Section 5 is conclusions.

2 Models

2.1 Hydrodynamic Model – FVCOM

FVCOM is a prognostic, unstructured grid, finite-volume coastal ocean and estuarine model. It was originally developed by Chen *et al.* (2003) and upgraded by joint efforts of scientists at University of Massachusetts-Dartmouth (UMASSD) and Woods Hole Oceanographic Institution (WHOI) (Chen *et al.*, 2006a, b; Chen *et al.*, 2007, Huang *et al.*, 2008). FVCOM is discretized with triangular grids in the horizontal and generalized terrain-following coordinate in the vertical. The model utilizes the modified Mellor and Yamada (1982) level 2.5 (MY-2.5) and Smagorinsky turbulent closure schemes as default setups for vertical and horizontal mixing, respectively, with an option for various turbulent parameterizations using the Generalized Ocean Turbulence Model (GOTM) (Burchard, 2002). FVCOM includes both hydrostatic and non-hydrostatic dynamics (Lai *et al.*, 2010a, b), and can be solved either by mode-split scheme or semi-implicit scheme. The current version of FVCOM used in this study includes wetting/drying treatment, 3D sediment module, ice module, *etc.* In a generalized terrain-following coordinate system, the governing equations of momentum, continuity, temperature, salinity, and density with the inclusion of three-dimensional radiation stress (Mellor 2003, 2005, 2008) are given as follows:

$$\frac{\partial uD}{\partial t}+\frac{\partial u^2D}{\partial x}+\frac{\partial uvD}{\partial y}+\frac{\partial u\omega}{\partial\hat{\sigma}}-fvD$$
$$=-D\frac{\partial}{\partial x}(g\eta+p_{atm})-D\int_{\hat{\sigma}}^{0}(D\frac{\partial b}{\partial x}-\varsigma\frac{\partial D}{\partial x}\frac{\partial b}{\partial\hat{\sigma}})d\hat{\sigma}$$
$$-(\frac{\partial DS_{xx}}{\partial x}+\frac{\partial DS_{xy}}{\partial y})+\hat{\sigma}(\frac{\partial D}{\partial x}\frac{\partial S_{xx}}{\partial\hat{\sigma}}+\frac{\partial D}{\partial y}\frac{\partial S_{xy}}{\partial\hat{\sigma}})+\frac{\partial\tau_x}{\partial\hat{\sigma}} \quad (1)$$

$$\frac{\partial vD}{\partial t}+\frac{\partial uvD}{\partial x}+\frac{\partial v^2D}{\partial y}+\frac{\partial v\omega}{\partial\hat{\sigma}}+fuD$$
$$=-D\frac{\partial}{\partial y}(g\eta+p_{atm})-D\int_{\hat{\sigma}}^{0}(D\frac{\partial b}{\partial y}-\varsigma\frac{\partial D}{\partial y}\frac{\partial b}{\partial\hat{\sigma}})d\hat{\sigma}$$
$$-(\frac{\partial DS_{xy}}{\partial x}+\frac{\partial DS_{yy}}{\partial y})+\hat{\sigma}(\frac{\partial D}{\partial x}\frac{\partial S_{xy}}{\partial\hat{\sigma}}+\frac{\partial D}{\partial y}\frac{\partial S_{yy}}{\partial\hat{\sigma}})+\frac{\partial\tau_y}{\partial\hat{\sigma}} \quad (2)$$

$$\frac{\partial Du}{\partial x}+\frac{\partial Dv}{\partial y}+\frac{\partial\omega}{\partial\hat{\sigma}}+\frac{\partial\eta}{\partial t}=0 \quad (3)$$

$$\frac{\partial\theta D}{\partial t}+\frac{\partial\theta uD}{\partial x}+\frac{\partial\theta vD}{\partial y}+\frac{\partial\theta\omega}{\partial\hat{\sigma}}=\frac{1}{D}\frac{\partial}{\partial\hat{\sigma}}(K_h\frac{\partial\theta}{\partial\hat{\sigma}})+D\hat{H}+DF_\theta \quad (4)$$

$$\frac{\partial sD}{\partial t}+\frac{\partial suD}{\partial x}+\frac{\partial svD}{\partial y}+\frac{\partial s\omega}{\partial\hat{\sigma}}=\frac{1}{D}\frac{\partial}{\partial\hat{\sigma}}(K_h\frac{\partial s}{\partial\hat{\sigma}})+DF_s \quad (5)$$

$$\rho=\rho(\theta,s), \quad (6)$$

where x, y and $\hat{\sigma}$ is the east, north and vertical axes of the generalized terrain-following coordinate; t the time; u, v , and ω the x, y and $\hat{\sigma}$ components of the velocity; τ_x and τ_y the x and y components of the stress; η the sea surface elevation; h the mean water depth; $D=h+\eta$ the total water depth; θ the potential temperature; s the salinity; ρ the density; p_{atm} the air pressure; f the Coriolis parameter; $\hat{H}$ the solar irradiance; and K_{h} the thermal vertical eddy diffusion coefficient; F_θ and F_s represent the thermal and salt diffusion terms. S_{xx}, S_{xy}, $S_{xy,}$ and S_{yy} are the x and y components of the radiation stress given as

$$S_{xx}=kE(\frac{k_xk_x}{k^2}F_{CS}F_{CC}-F_{SC}F_{SS})+E_D,$$
$$S_{yy}=kE(\frac{k_yk_y}{k^2}F_{CS}F_{CC}-F_{SC}F_{SS})+E_D,$$
$$S_{xy}=kE\frac{k_xk_y}{k^2}F_{CS}F_{CC},$$

where E is the wave energy computed by

$$E=\frac{1}{16}gHs^2,$$

and

$$F_{SC}=\frac{\sinh k(z+h)}{\cosh kD},\ F_{CC}=\frac{\cosh k(z+h)}{\cosh kD},$$

$$F_{SS}=\frac{\sinh k(z+h)}{\sinh kD},\ F_{CS}=\frac{\cosh k(z+h)}{\sinh kD},$$

$$E_D=0,\ \text{if}\ z\neq\eta\ \text{and}\ \int_{-h}^{\eta+}E_D\mathrm{d}z=E/2$$

Hs, k, k_x, and k_y are the significant wave height, wave number, wave number in x direction, wave number in y direction, respectively.

The original surface and the bottom stresses are computed by the drag equation (proportional to quadratic velocity) but in the coupled model they are related to wave and sediment and more detail will be presented in Section 3.1.

2.2 Wave Model

The wave model FVCOM-SWAVE, developed by Qi *et al.* (2009), is an unstructured-grid, finite-volume version of SWAN. The governing equation for wave action density (N) in FVCOM-SWAVE is given as

$$\frac{\partial N}{\partial t}+\frac{\partial c_x N}{\partial x}+\frac{\partial c_y N}{\partial y}+\frac{\partial c_\sigma N}{\partial \sigma}+\frac{\partial c_{\hat{\theta}} N}{\partial \hat{\theta}}=\frac{S_{tot}}{\sigma}, \quad (7)$$

where $(\sigma, \hat{\theta})$ is the relative frequency and wave direction in spectral space; (x, y) is the Cartesian coordinate in geographic space. S_{tot} is the source/sink term representing the effects of wind-wave generation, wave breaking, bottom dissipation, and nonlinear wave-wave interactions (Booij *et al.*, 2004; Qi *et al.*, 2009).

Qi *et al.*'s study (2009) provided the detail descriptions of the discrete algorithms in FVCOM-SWAVE. The wave action density in Eq.7 was solved numerically by four integral steps: the variations of action density spectrum in spectral space, frequency and direction, respectively, the wave propagation in geographic space, and the growth, transfer and decay of waves. The wave propagation in geographic space was solved with either an explicit or a semi-implicit finite-volume upwind advection scheme.

2.3 Sediment Transport Model

The sediment transport model in FVCOM (called FVCOM-SED) is based on the Community Sediment Transport Model (CSTM) (Chen *et al.*, 2006b). Sediment transport is calculated by solving the advection-diffusion equation with vertical settling and exchange with bed as the source and sink terms. The general form of the source and sink terms can be written as

$$C_{source}=-\frac{\partial w_{s,m} C_m}{\partial s}+E_{s,m}, \quad (8)$$

where $w_{s,m}$ is the vertical-settling velocity (positive upwards), C_m the quantity of suspended sediment, $E_{s,m}$ the erosion source, and m the number of sediment classes. The model solves each term of the advection-diffusion equation in the following sequence: vertical settling, source and sink, horizontal advection, vertical advection, vertical diffusion, and finally horizontal diffusion (Chen *et al.*, 2006b). A bottom-boundary layer model with the wave-current interactions and morphology feedback is added into FVCOM-SED to couple FVCOM-SED, FVCOM-SWAVE, and FVCOM. The algorithms for erosion, deposition, and bedload transport with and without waves were described in detail by Warner *et al.* (2008).

3 Model Coupling

3.1 Circulation Model

3.1.1 Radiation stress

Three-dimensional radiation stress is implemented in the momentum equations (Eqs. 1 and 2) and is associated with the wave-induced nearshore circulation and wave setup.

3.1.2 Bottom boundary layer

The wave-induced high-frequency (with a period of about 10 s) oscillatory shear in a thin (a few centimeters) wave-boundary layer not only produces turbulence mixing, but also large shear stresses. Turbulence enhances the momentum transfer and the interaction between the dynamic processes in water column and bottom boundary layer, and thus intensifies frictional drag exerted on mean flow. Shear stress induces sediment resuspension and enhances bedload transport. The change of the seabed due to sediment transport can form ripples and other bedforms. In turn, the bottom roughness can modify the vertical shear of the mean flow. Bedload transport can also induce drag on the flow, because momentum is transferred to particles as they are removed from the bed and accelerated by the flow. Resuspended sediments can produce sediment-induced stratification. When the sediment is at a high concentration, this process can change the effective viscosity of the fluid (Warner *et al.*, 2008).

The code of the bottom boundary layer (BBL) with inclusion of the wave-current-sediment interaction was developed and implemented in ROMS by Warner *et al.* (2008). The same scheme was converted into FVCOM.

3.1.3 Calculation of surface stress

The sea surface roughness is calculated as follows (Donelan, 1993):

$$Z_0=3.7\times10^{-5}\frac{U_{10}^2}{g}\left(\frac{U_{10}}{C_p}\right)^{0.9}, \quad (9)$$

where Z_0 is the sea surface roughness, C_p the phase velocity of the peak frequency and U_{10} the 10 m wind speed. The wave age is given by U_{10}/C_p.

The drag coefficient is

$$C_d=\left(\alpha/\ln(10/Z_0)\right)^2, \quad (10)$$

where α(=0.41) is the von Kármán constant.

The surface stress can be obtained by

$$\tau=\rho_a C_d U_{10}^2, \quad (11)$$

where ρ_a is the air density. U_{10} is calculated as the apparent wind, *i.e.*, the wind speed relative to current.

3.2 Wave Model

FVCOM-SWAVE solves the wave-action density equation. In the coupling system, wind, current, sea surface elevation and depth change are provided to the wave model. The current is depth-averaged and weighted by wave parameters (Mellor, 2008). In the terrain-following coordinates, it is expressed by

$$u_{A\alpha}=kD\int_{-1}^{0}U_\alpha[(F_{CS}F_{CC}+F_{SS}F_{SC})/2+F_{CS}F_{SS}]\mathrm{d}\hat{\sigma}. \quad (12)$$

3.3 Morphology

Morphology dynamics becomes important in coastal regions where seabed is not stable and sediment move-

ment is significant. Morphological changes can have significant influence on flow and transport. In the coupled model system, the changes are accounted for by equating the bottom-boundary condition of the vertical velocity to the rate of change of elevation of the sea floor. This method guarantees the mass conservation. A morphological scale factor is adopted to accelerate long-term simulations. A value of one has no effect, and values greater than one accelerate the bed response (Roelvink, 2006).

3.4 The Coupling Procedure

The same time step is used for each model. To obtain more accurate calculations of nonlinear interactions, the model coupling is performed for every time step. The coupling system is illustrated in Fig.1.

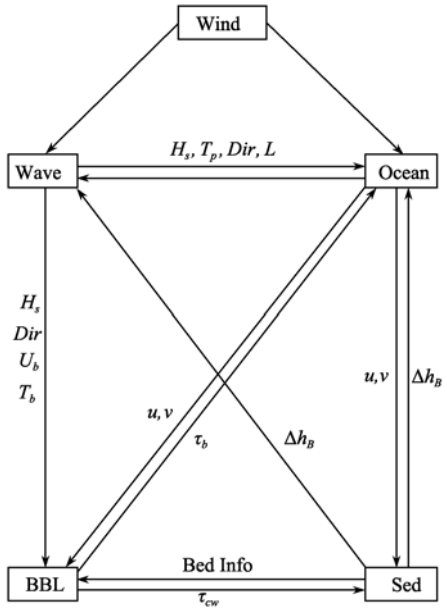

Fig.1 Coupling between FVCOM circulation model (OCEAN), FVCOM wave model (WAVE), and FVCOM sediment model (SED) through BBL, the bottom boundary layer model.

After the initialization, the wave model starts to calculate significant wave height (H_s), wave direction (*Dir*), average wave length (L), surface wave relative peak period (T_p), wave bottom orbit velocity (U_b), and bottom wave period (T_b). The radiation stress or surface stress is passing to the circulation model that starts after the wave model. The results of current and surface elevation from the circulation model are the feedback to the wave model for the wave calculation of the next time step. The sediment transport model starts after the ocean model. The morphological change due to the sediment movement is used to update the depths of both the wave and ocean model. After the three models finish the calculation, wave parameters, current fields and bed parameters are sent to the BBL model, which then provides the bottom stresses under the combined influence of waves, currents, and sediment transport. These stresses will be used in the ocean model to solve the momentum equation and in the sediment transport model to calculate suspended load and bedload transport. Thus a dynamic coupling cycle of waves, currents, and sediment transport is completed.

4 Validation Experiments

Two benchmark experiments were conducted to validate the coupled system. Both cases were carried out for a rectangular computational domain. The first is a plane beach case aimed to evaluate the accuracy of the radiation stress calculation, and the wave-induced setup and currents, and the second is a tidal inlet case aimed to examine the effect of current-wave interactions on sediment distributions around the exit of the inlet. For the first case, the results of an analytical solution and the measuring data from a laboratory experiment were used to validate the coupled model. For the second case, a comparison with ROMS was made to check if the unstructured grid coupled model can provide the same accurate results as the structured grid coupled model in the same configuration for simple geometric domain. The comparison made here focused on the current-wave-sediment interactions. Huang *et al.* (2008) found that FVCOM has the faster convergence rate to the analytical solution comparing to ROMS for the same cases in this study. If FVCOM has the same accuracy as ROMS in the rectangular domain, the geometric flexibility of FVCOM will provide a more suitable tool for realistic coastal and estuarine regions where the coastline is characterized by irregular geometry.

4.1 The Plane Beach Case

Following Xia *et al.* (2004), we considered a case of normally incident waves approaching a plane beach with a slope of 1:10. There exists an analytical solution for the wave setup and the laboratory result describing vertical current profiles in a similar case.

Longuet-Higgins and Stewart (1964) gave an analytical solution of the wave set-up on a sloping beach with a straight coastline when the shore-normal waves come nearshore. The assumptions are as follows:

$$\frac{\mathrm{d}S_{xx}}{\mathrm{d}x}=-\rho gD\frac{\mathrm{d}\zeta}{\mathrm{d}x}, \tag{13}$$

$\mathrm{d}(EC_g)/\mathrm{d}x=0$ outside the surf zone, where C_g is the group speed; inside the surf zone the wave height $H=rD$, where $r=0.83$. Under these assumptions, the wave setdown appears outside the surf zone and setup appears inside the surf zone with the functions

$$\zeta=-\frac{H^2k}{8\sinh 2kD} \tag{14}$$

and

$$\zeta=(1+\frac{8}{3r^2})^{-1}(D_B-D)+\zeta_B \tag{15}$$

respectively, where D_B and ζ_B are the water depth and the value of wave set-down at the breaking point. Bijker *et al.*

(1974) measured the vertical current profile on a beach with different slope under various wave conditions. Here their 'wave 5' is chosen and the corresponding parameters are listed in Table 1.

Table 1 Model parameters for the plane beach test case

Model parameter	Value
Length (cross-shore)	9 m
Width (longshore)	0.433 m
Offshore depth	0.45 m
Beach splope	1/10
Number of sigma layers	8
Grid size	0.125 m
Time step	0.0005 s
Duration	Until steady
Offshore wave height	0.181 m
Wave period	1.5 s
Bottom stress formulation	Quadratic
Bottom friction factor	0.0015 m

Fig.2 is the comparison of water surface elevation between the model results and the analytical solution by Eqs. (14) and (15). The model results agree well with the analytical solution. From the figure we can also see that outside the breaking point the waves cause the water level to decrease from offshore towards this point, and inside the surf zone the waves cause the water level to increase linearly from the breaking point to the shoreline. Xia *et al.* (2004) speculated that the slightly difference between their model results and analytical solutions are due to the omission of bottom stress in Eq. 13. We tried to remove the bottom stress in the coupled model but found it has little influence on the calculated set-up. Further study shows that the horizontal or vertical mixing coefficient, often influenced by wave mixing, plays an important role in modeling the wave induced set-up.

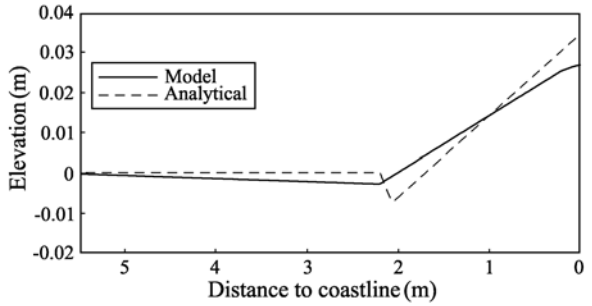

Fig.2 Wave-induced setup or setdown.

The vertical profile of calculated currents is shown in Fig.3. Two circulation gyres are formed in the vertical section. Outside the surf zone the circulation is clockwise and inside the surf zone counter-clockwise. This circulation pattern and the order of the current magnitude agree well with Bijker's laboratory experiment.

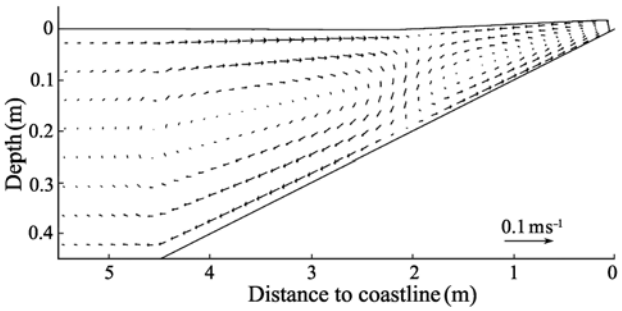

Fig.3 Wave-induced current inside and outside the surf zone.

4.2 The Tidal Inlet Case

Consider a semi-enclosed rectangular basin with a width of 15 km and a length of 14 km. The initial water depth is specified as 4 m at the southern end and linearly increases to 15 m at the northern end where the open boundary is located. A wall with a 2-km center opening is placed across the middle of the basin (Fig.4). The model is forced by oscillating water level with an amplitude of 1 m at the open boundary. Waves with 1-m height and 10-s period are also imposed at the open boundary and propagate nearshore. Parameters used to drive the coupled model are listed in Table 2.

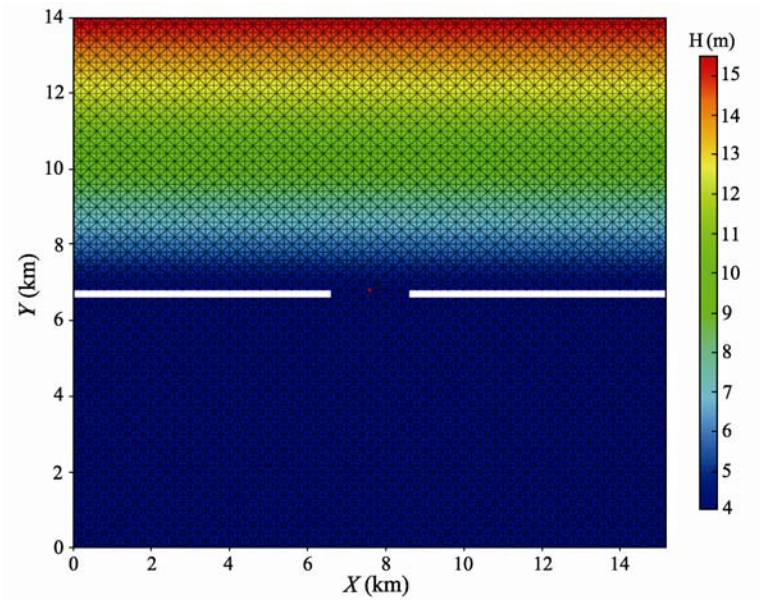

Fig.4 Model grid and initial bathymetry.

Table 2 Model parameters

Parameters	Value
Length, width, depth	15 km, 14 km, 4 m
Nodes, elements, sigma layers	5467, 10508, 8
Simulation time	2 d
Initial condition	Cold start
	H_s=1 m, T_p=10 s
Open boundary condition	Tidal amplitude=1 m,
	Period=12 h
Median grain diameter	0.1 mm
Sediment density	2650 kg m^{-3}
Settling velocity	11 mm s^{-1}
Erosion rate	0.005 kg m^{2} s^{-1}
Critical stress	0.1 Pa
Porosity	0.5
Morphology factor	10
Bed thickness	10 m
Bottom roughness	0.0015 m

4.2.1 Morphology

The model simulations are conducted for a 2-day period with a morphologic scale factor of 10. Fig.5 shows the bed thickness predicted by ROMS and the present coupled model. Both models predict the same pattern of the bed change, but the detail spatial distributions of the thickness differ. To examine what could cause these differences, we have run both ROMS and FVCOM. The results suggest that the differences are due to 1) different open boundary treatments and 2) modifications made in ROMS and SWAN. We found that in ROMS, when the tidal forcing at the open boundary is removed, SWAN shows a free-friction pattern that is different from the original SWAN. The drag forcing modification made in ROMS for the wave component seems not proper for the case when the hydrodynamic process is shut down.

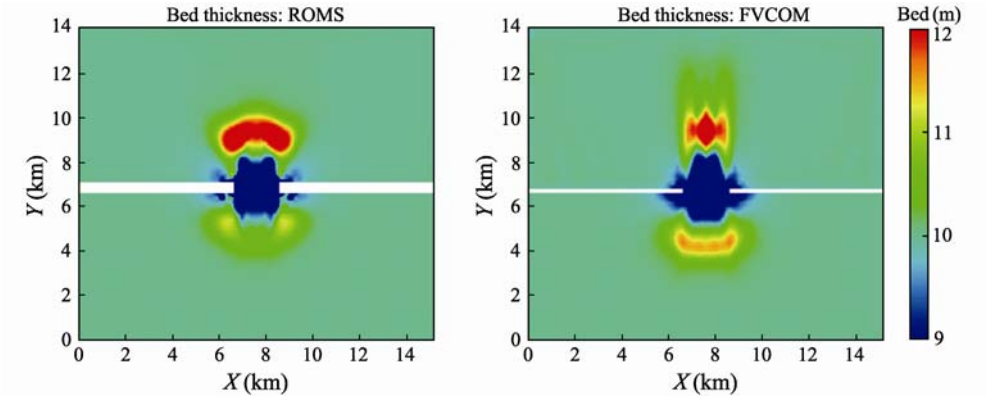

Fig.5 Bed thickness after two-day simulations.

4.2.2 Wave results

Under the same conditions, the predicted waves by the FVCOM coupled system are identical to those by the original SWAN. The wave heights evolve to a steady state, decreasing southward toward the inlet (Fig.6).

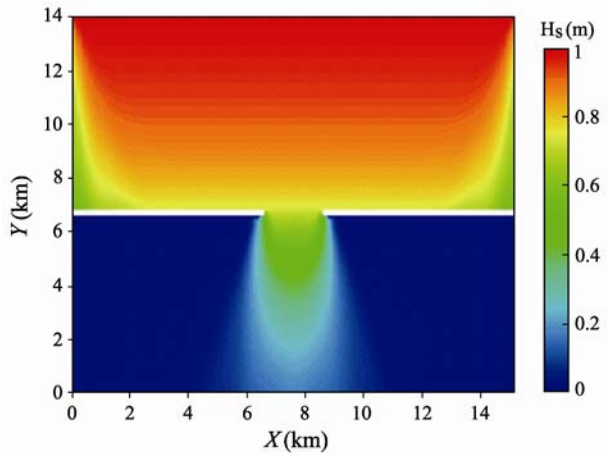

Fig.6 Significant wave height field.

When coupled to the hydrodynamic model, the current-wave interaction changes the nature of waves and no steady state exists anymore. To illustrate it, we plot the time series of wave height and current velocity at Point A, the center of the inlet.

Fig.7 shows the time series of wave height for the cases with and without current-wave interaction. In the case without the current-wave interaction, the wave height has a constant value close to 0.8 m. When currents are included, the nonlinear interaction of currents and waves

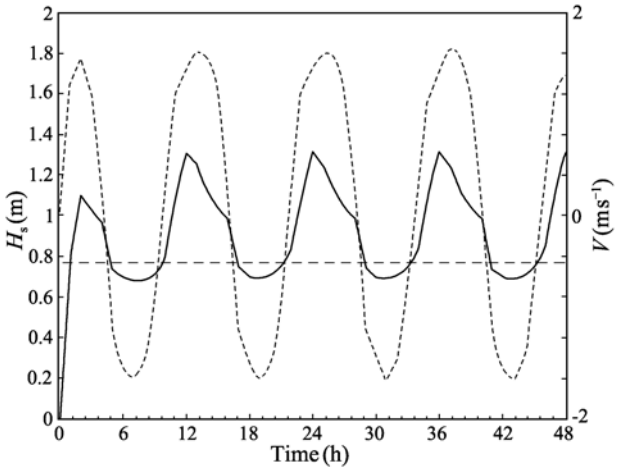

Fig.7 Wave height and y component velocity at Point A. Solid line designates wave height computed with the coupled model, dash-dotted line y component velocity, and dashed line wave height computed with the wave model only.

causes a periodic variation of the wave height with the same period as the tidal currents. Fig.7 also qualitatively confirms that wave energy increases in a direction opposite to current and decreases in the same direction as the current due to changes in group velocity. This result is consistent with the previous findings by Tolman (1990).

4.2.3 Current results

Three factors in the coupling model can influence the currents: radiation stress, bottom stress, and bathymetry change. Fig.8 is a snapshot of the current field calculated by FVCOM with and without current-wave-sediment coupling. At ebb tide, two eddies calculated by the coupled model are slightly smaller and further away from the inlet comparing to those by the non-coupled FVCOM. The water level field calculated by the coupled model is much smoother than that by the non-coupled model at ebb tide.

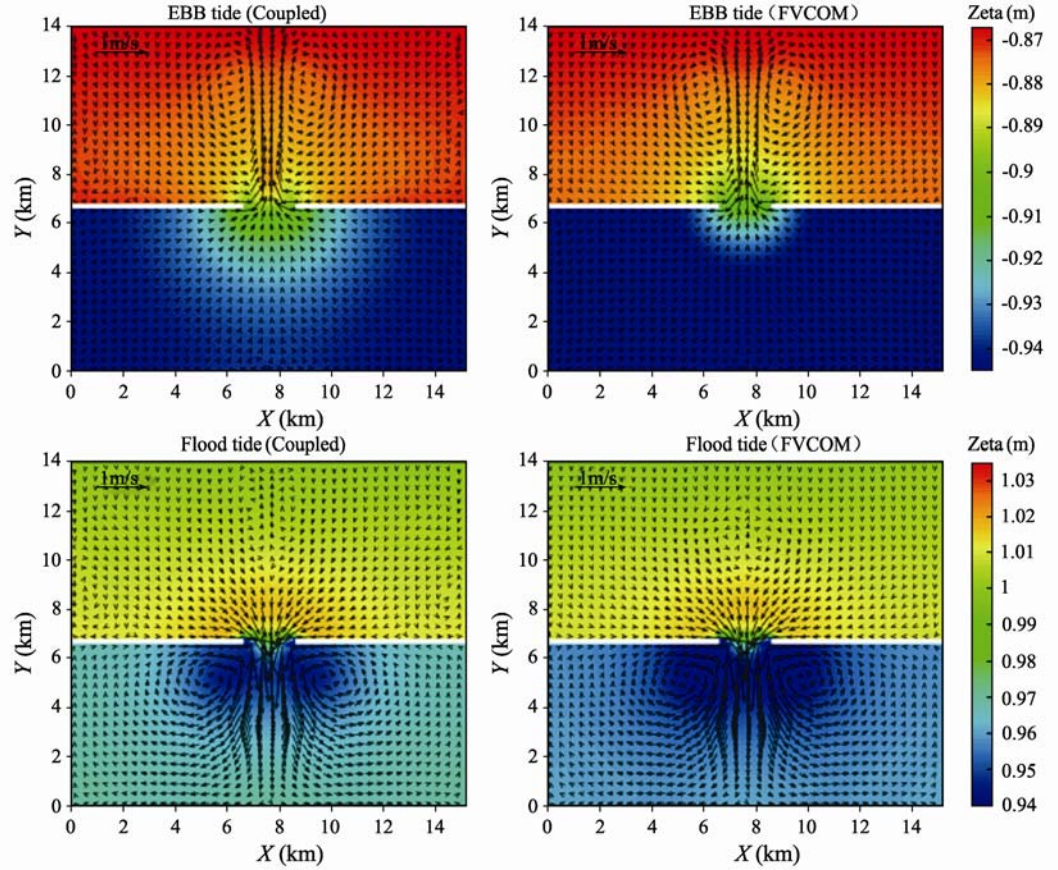

Fig.8 Current and water level fields calculated by the coupled system and the non-coupled FVCOM.

5 Conclusions

In this study, an effort was made to couple FVCOM-SWAVE and FVCOM-SED with FVCOM to form a three dimensional fully coupled wave-current-sediment model system. Using the same unstructured grid for the hydrodynamics, waves, and sediment transport models, the coupling algorithm does not require any interpolations from one to another, which ensures the mass conservation and correct energy transfer within the system.

Two benchmark tests are used to validate the model. For the plane beach case, the calculated results agree well with the analytical solution and the laboratory experiment. For the tidal inlet case, the coupling between waves, currents and sediment as well as the bathymetry change has been demonstrated and the FVCOM results compared with ROMS'. Both models show the same bed thickness patterns but detailed distributions differ. The differences are due to the parameterizations for the current-wave interactions. Clearly more comparisons with observations are required to further evaluate the coupled modeling system.

In summary, the FVCOM-based coupling of the wave, current, and sediment transport model is accomplished and validations of the system are conducted by comparing the model results with the analytical solutions, the laboratory data, and the existing coupled model. The further validations and applications of the system are underway and will be published in separate papers.

Acknowledgements

The first author is supported by the State Scholarship Fund for his PhD degree during a two-year (2007-2009) study at University of Massachusetts-Dartmouth in US.

References

Bijker, E. W., Kalwijk, J. P. Th., and Pieters, T., 1974. Mass transport in gravity waves on a sloping bottom. *Proc. 14th*

Conf. Coastal Engineering, vol. 2. ASCE, New York, 447-465.

Booij, N., Haagsma, I. J. G., Holthuijsen, L. H., Kieftenburg, A. T. M. M., Ris, R. C., van der Westhuysen, A. J., and Zijlema, M., 2004. SWAN Cycle III version 40.51 User Manual. Delft University of Technology, Available: http://fluidmechanics.tudelft.nl/swan/index.htm.

Burchard, H., 2002. *Applied Turbulence Modeling in Marine Waters*. *Lecture Notes in Earth Sciences*, Springer: Berlin-Heidelberg-New York-Barcelona-Hong Kong-London-Milan Paris-Tokyo, 215pp.

Chen, C. S., Liu, H. D., and Beardsley, R. C., 2003. An unstructured grid, finite-volume, three-dimensional, primitive equation ocean model: application to coastal ocean and estuaries. *Journal of Atmospheric and Oceanic Technology*, **20**: 159-186.

Chen, C. S., Beardsley, R. C., and Cowles, G., 2006a. An unstructured grid, finite-volume coastal ocean model–FVCOM user manual, School for Marine Science and Technology, University of Massachusetts Dartmouth, New Bedford, Second Edition. Technical Report SMAST/UMASSD-06-0602, 318pp.

Chen, C. S., Beardsley, R. C., and Cowles, G., 2006b. An unstructured grid, finite-volume coastal ocean model (FVCOM) system. Special Issue: *Advance in Computational Oceanography*, *Oceanography*, **19** (1): 78-89.

Chen, C. S., Huang, H. S., Beardsley, R. C., Liu, H. D., Xu, Q. C., and Cowles, G., 2007. A finite-volume numerical approach for coastal ocean circulation studies: comparisons with finite difference models. *Journal of Geophysical Research*, **112**, C03018. DOI: 10.1029/2006JC003485.

Donelan, M. A., Dobson, F. W., and Smith, S. D., 1993. On the dependence of sea surface roughness on wave development. *Journal of Physical Oceanography*, **23**: 2143-2149.

Grant, W. D., and Madsen, O. S., 1979. Combined wave and current interaction with a rough bottom. *Journal of Geophysical Research*, **84** (C4): 1797-1808.

Haidvogel, D. B., Arango, H., Budgell, W. P., Cornuelle, B. D., Curchitser, E., Di Lorenzo, E., Fennel, K., Geyer, W. R., Hermann, A. J., Lanerolle, L., Levin, J., McWilliams, J. C., Miller, A. J., Moore, A. M., Powell, T. M., Shchepetkin, A. F., Sherwood, C. R., Signell, R. P., Warner, J. C., and Wilkin, J., 2008. Ocean forecasting in terrain-following coordinates: Formulation and skill assessment of the Regional Ocean Modeling System. *Journal of Computational Physics*, **227**: 3595-3624.

Huang, H. S., Chen, C. S., Cowles, G. W., Winant, C. D., Beardsley, R. C., Hedstrom, K. S., and Haidvogel, D. B., 2008. FVCOM validation experiments: comparisons with ROMS for three idealized barotropic test problems. *Journal of Physical Oceanography*, **113**, C07042. DOI: 10.1029/2007JC004557.

Lai, Z. G., Chen, C. S., Cowles, G., and Beardsley, R. C., 2010a. A non-hydrostatic version of FVCOM, Part I: validation experiment. *Journal of Geophysical Research*, 115. DOI: 10.1029/2009JC005525.

Lai, Z. G., Chen, C. S., Cowles, G., and Beardsley, R. C., 2010b. A non-hydrostatic version of FVCOM, Part II: mechanistic study of tidally generated nonlinear internal waves in Massachusetts Bay. *Journal of Geophysical Research*. DOI: 10.1029/2010JC006331.

Liang, B. C., Li, H. J., and Lee, D. Y., 2007. Numerical study of three-dimensional suspended sediment transport in waves and currents. *Ocean Engineering*, **34**: 1569-1583.

Liu, H. Q., and Xie, L. A., 2009. A numerical study on the effects of wave-current-surge interactions on the height and propagation of sea surface waves in Charleston Harbor during Hurricane Hugo 1989. *Continental Shelf Research*, **29**: 1454-1463.

Longuet-Higgins, M. S., and Stewart, R. W., 1960. Changes in the form of short gravity waves on long waves and tidal currents. *Journal of Fluid Mechanics*, **8**: 565-583.

Longuet-Higgins, M. S., and Stewart, R. W., 1964. Radiation stress in water waves: a physical discussion with applications. *Deep Sea Research*, **11**: 529-562.

Longuet-Higgins, M. S., 1970a. Longshore currents generated by obliquely incident sea waves, 1. *Journal of Geophysical Research*, **75** (33): 6778-6789.

Longuet-Higgins, M. S., 1970b. Longshore currents generated by obliquely incident sea waves, 2. *Journal of Geophysical Research*, **75** (33): 6790-6801.

Mellor, G. L., and Yamada, T., 1982. Development of a turbulence closure model for geophysical fluid problem. *Reviews of Geophysics and Space Physics*, **20**: 851-875.

Mellor, G. L., 2003. The three-dimensional current and surface wave equations. *Journal of Physical Oceanography*, **33**: 1978-1989.

Mellor, G. L., 2005. Some consequences of the three-dimensional currents and surface wave equations. *Journal of Physical Oceanography*, **35**: 2291-2298.

Mellor, G. L., 2008. The Depth-Dependent Current and Wave Interaction Equations: A Revision. *Journal of Physical Oceanography*, **38**: 2587-2596.

Moon, I. J., 2005. Impact of a coupled ocean wave-tide-circulation system on coastal modeling. *Ocean Modelling*, **8**: 203-236.

Qi, J. H., Chen, C. S., and Beardsley, R. C., 2009. An unstructured-grid finite-volume surface wave model (FVCOM-SWAVE): Implementation, validations and applications. *Ocean Modelling*, **28**: 153-166.

Roelvink, J. A., 2006. Coastal morphodynamic evolution techniques. *Coastal Engineering*, **53**: 277-287.

Sørensen Ole, R., Henrik Kofoed-Hansen and Jones Oliver P. 2006. Numerical modeling of wave-current interaction in tidal areas using an unstructured finite volume technique. Proceedings of the 30th International Conference of Coastal Engineering 2006, San Diego, California, USA. **1**: 653-665.

Tang, H. S., Keenb, T. R., and Khanbilvardi, R., 2009. A model-coupling framework for nearshore waves, currents, sediment transport, and seabed morphology. *Communications in Nonlinear Science and Numerical Simulation*, **14** (7): 2935-2947.

Tolman, H. L., 1990. The influence of unsteady, depths and currents of tides on wind-wave propagation in shelf seas. *Journal of Physical Oceanography*, **20**: 1166-1174.

Warner, J. C., Sherwood, C. R., Signell, R. P., Harris, C., and Arango, H. G., 2008. Development of a three-dimensional, regional, coupled wave, current, and sediment-transport model. *Computers and Geosciences*, **34**: 1284-1306.

Xia, H. Y., Xia, Z. W., and Zhu, L. S., 2004. Vertical variation in radiation stress and wave-induced current. *Coastal Engineering*, **51**: 309-321.

Xie, L. A., Wu, K. J., and Pietrafesa, L., and Zhang, C., 2001. A numerical study of wave–current interaction through surface and bottom stresses: Wind-driven circulation in the South Atlantic Bight under uniform winds. *Journal of Geophysical Research*, **106** (C8): 16 841-16 855.

(Edited by Xie Jun)